ChemPubSoc Europe

DOI: 10.1002/cssc.202000094

CHEMSUSCHEM Communications



# A Quinone Anode for Lithium-Ion Batteries in Mild Aqueous Electrolytes

Yan Jing,[a, c] Yanliang Liang,[a] Saman Gheytani,[a] and Yan Yao*[a, b]

Aqueous batteries could be potentially used for grid-scale energy storage owing to the use of nonflammable electrolytes and long cycle life. Recently, quinones have shown examples as redox-active materials in aqueous batteries under either strong acidic or basic conditions. However, a quinone-based battery with a less corrosive electrolyte is still rare. Given that quinone-based batteries are heavily influenced by the pH of electrolytes, we studied the influence of acid dissociation constants (p*K*a) of hydroquinones on their performance as solid electrode materials. We measured the p*K*a of anthracene-9,10-diol ($AQH_2$) and benzo[1,2-b:4,5-b′]dithiophene-4,8-diol ($BDTDH_2$) from the Pourbaix diagrams of two *para*-quinone monomers [i.e., anthracene-9,10-dione (AQ) and benzo[1,2-b:4,5-b′]dithiophene-4,8-dione (BDTD)]. Subsequently, their polymeric forms [i.e., poly(anthraquinonyl sulfide) (PAQS) and poly(benzo[1,2-b:4,5-b′]dithiophene-4,8-dione-2,6-diyl sulfide) (PBDTDS)] were investigated as electrodes in aqueous lithium-ion cells. At pH 13, PAQS demonstrates a low capacity and poor cycle life, whereas PBDTDS shows a capacity of 196 mAh g$^{-1}$ and fade rates of 0.0038% per cycle over 4200 cycles, 0.77% per day over 21 days. The differences in capacity and cycle stability can be explained by the difference of corresponding p*K*a values. A full cell with the configuration of (−)PBDTDS | 2.5 M $Li_2SO_4$ (pH 13) | $LiCoO_2$(+) shows a voltage of 1.08 V, a capacity of 72 mAh g$^{-1}$ and ≈99.9% of Coulombic efficiency for 500 stable cycles.

## Introduction

With electricity increasingly generated from renewable resources such as solar and wind power, energy storage devices have become more and more indispensable in balancing the electricity supply and demand.[1–8] Aqueous lithium-ion batteries (ALIBs), featuring safety and long cycle life, could become a viable option serving as energy storage devices.[9–12] Developing robust electrode materials for ALIBs is thus becoming paramount. Compared to cathode choices such as $LiFePO_4$,[13] $LiCoO_2$,[14] $LiMn_2O_4$,[15] and Prussian blue analogues,[16] which have demonstrated excellent cycle stability in aqueous electrolytes, high performance anodes for ALIBs are still less common.[10,17,18]

In ALIBs, carbon-coated $LiTi_2(PO_4)_3$ anode shows ≈103 mAh g$^{-1}$ and 90% of capacity retention after 1000 cycles.[19,20] In comparison, organic-based anodes demonstrate higher capacity and better stability.[21–23] For example, polyimides show up to 150 mAh g$^{-1}$ of capacity and over 90% of capacity retention even after thousands cycles.[24] However, it has been reported that redox-active imides can hydrolyze at high pH and are limited for use at neutral pH to achieve a long cycle life.[25–27] Quinones have shown great structural stability in both acidic and alkaline solutions.[20–30] Their structural diversity and tunability further allow property-oriented molecular design toward high-performance electrodes.[22,31] We recently reported an *ortho*-quinone-based polymer (PPTO) anode for ALIBs and demonstrated the highest capacity of 229 mAh g$^{-1}$ with excellent cycle stability at neutral pH.[18] The excellent electrochemical performance demonstrated by *ortho*-quinones inspired us to further explore *para*-quinones. Despite the well-established electrochemistry of *para*-quinones in aqueous solutions[29] and the use in flow batteries,[2,27,32,33] the use of *para*-quinones as solid form anodes in ALIBs has not yet been reported.[34]

Starting with two *para*-quinone-based monomers [i.e., anthraquinone (AQ) and benzo[1,2-b:4,5-b′]dithiophene-4,8-dione (BDTD)], we investigated their redox potentials within a broad buffered pH range and were able to plot their Pourbaix diagrams and identify the acid dissociation constants (p$Ka_1$, p$Ka_2$) of the two corresponding *para*-hydroquinone derivatives [i.e., anthracene-9,10-diol ($AQH_2$) and benzo[1,2-b:4,5-b′]dithiophene-4,8-diol ($BDTDH_2$)]. To avoid the dissolution issue of quinone monomers in aqueous electrolytes, their polymeric forms were synthesized and evaluated as anodes in aqueous electrolytes. Owing to the higher p*K*a values of $AQH_2$, poly(anthraquinonyl sulfide) (PAQS) demonstrates low capacity and poor cycle stability when the pH is less than 14. Because of lower p$Ka_2$ of $BDTDH_2$, poly(benzo[1,2-b:4,5-b′]dithiophene-4,8-dione-

[a] Dr. Y. Jing, Dr. Y. Liang, Dr. S. Gheytani, Prof. Y. Yao
Department of Electrical and Computer Engineering and Materials Science and Engineering Program
University of Houston
4726 Calhoun Rd, Houston, TX 77204 (USA)
E-mail: yyao4@uh.edu

[b] Prof. Y. Yao
Texas Center for Superconductivity at the University of Houston
3369 Cullen Blvd, Houston, TX 77204 (USA)

[c] Dr. Y. Jing
Current address:
Department of Chemistry and Chemical Biology
Harvard University
12 Oxford Street
Cambridge, MA 02138 (USA)

Supporting Information and the ORCID identification number(s) for the author(s) of this article can be found under: https://doi.org/10.1002/cssc.202000094.

This publication is part of a Special Issue focusing on "Organic Batteries". A link to the issue's Table of Contents will appear here once it is complete.

2,6-diyl sulfide) (PBDTDS) shows a high capacity of 196 mAh g$^{-1}$ and 84% of capacity retention over 4200 cycles in 2.5 M $Li_2SO_4$ in a mild electrolyte of pH 13. A full cell with the configuration of PBDTDS | 2.5 M $Li_2SO_4$ (pH 13) | $LiCoO_2$ (Figure 1) exhibits a voltage of 1.08 V and a specific capacity of 72 mAh g$^{-1}$ (based on the combined mass of cathode and anode) as well as ≈99.9% Coulombic efficiency.

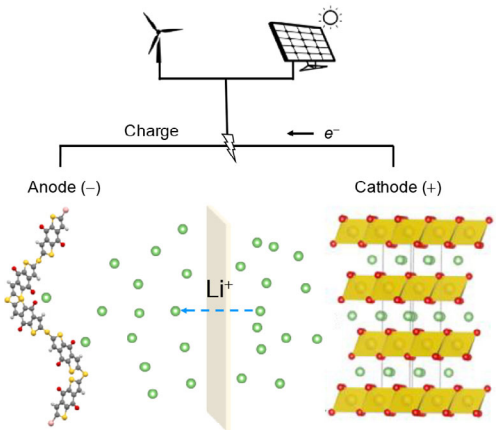


**Figure 1.** Scheme for an ALIB. Anode: PBDTDS. Cathode: $LiCoO_2$. Electrolyte: 2.5 M $Li_2SO_4$ (pH 13).

## Results and Discussion

BDTD and AQ are two selected *para*-quinones for electrochemical evaluations in buffered solutions. As shown in Figure 2, BDTD comprises a *para*-benzoquinone fused with two thiophene rings, AQ comprises a *para*-benzoquinone fused with two benzene rings. Such distinction in structure renders a 300 mV of difference in their reduction potentials in non-aqueous lithium batteries (2.5 V vs. Li/Li$^+$ for BDTD and 2.2 V vs. Li/Li$^+$ for AQ).[35] The difference in potentials was confirmed in the Pourbaix diagram shown in Figure 2a, where the relationship of potential and pH was extracted using differential pulse voltammetry technique (Figure S1). Furthermore, from the diagram, we can extract the acid dissociation constants (i.e., p$Ka_1$, p$Ka_2$) of $BDTDH_2$ and $AQH_2$. The plots with different slopes (from left to right: 59, 29, 0 mV/pH) create three pH regions, where the dominating species are $BDTDH_2$/$AQH_2$ for pH < p$Ka_1$, $BDTDH^-$/$AQH^-$ for p$Ka_1$ < pH < p$Ka_2$, and $BDTD^{2-}$/$AQ^{2-}$ for p$Ka_2$ < pH, respectively. Figure 2b and 2c illustrate the corresponding electrochemical reduction pathways in different pH ranges and the chemical reaction equilibria at p$Ka_1$ and p$Ka_2$. When pH < p$Ka_1$, BDTD and AQ will be electrochemically reduced to $BDTDH_2$ and $AQH_2$. When p$Ka_1$ < pH < p$Ka_2$, BDTD and AQ will be electrochemically reduced to $BDTDH^-$ and $AQH^-$. When p$Ka_2$ < pH, BDTD and AQ will be electrochemically reduced to $BDTD^{2-}$ and $AQ^{2-}$. When pH = p$Ka_1$, the first chemical equilibrium forms, where $[BDTDH_2]/[BDTDH^-] = 1$ and $[AQH_2]/[AQH^-] = 1$. When pH = p$Ka_2$, the second chemical equilibrium forms, where $[BDTDH^-]/[BDTD^{2-}] = 1$ and $[AQH^-]/[AQ^{2-}] = 1$. However, to build a rocking-chair type ALIB, one should choose pH of an electrolyte wisely to avoid the influence of proton-coupled electron-transfer process.

Two criteria should be considered when designing organic molecule-based anodes for ALIBs. First, the reduction potentials of molecules should be close to, but not lower than, that

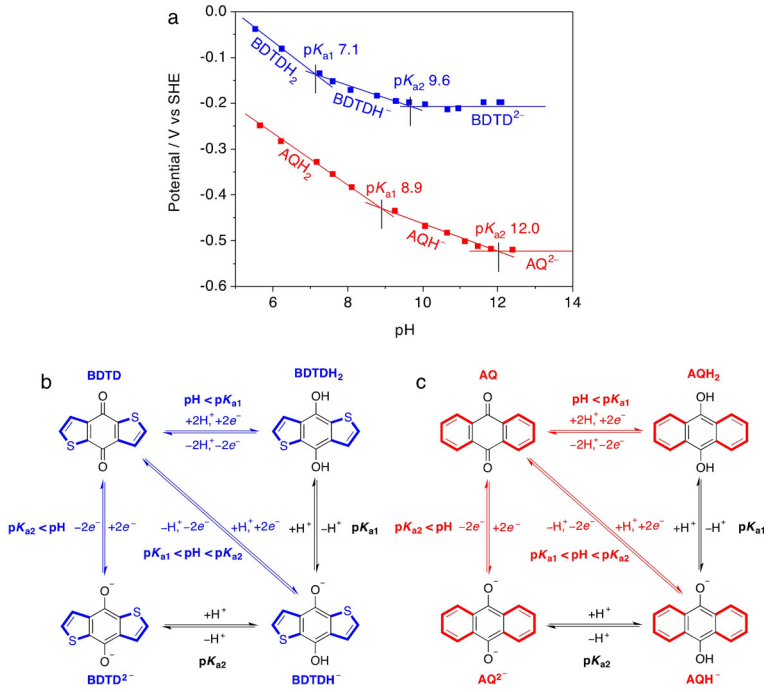


**Figure 2.** Determination of p*Ka* values for $BDTDH_2$ and $AQH_2$, and corresponding chemical equilibrium, electrochemical reduction reactions at different pHs. (a) Pourbaix diagram (potential vs. pH) of $BDTDH_2$ and $AQH_2$ in buffered electrolytes at room temperature. The lines are guides to the eye, and the slopes are ≈59, 29, and 0 mV per pH. (b,c) Electrochemical reductions of BDTD and AQ within different pH ranges, and chemical equilibria when the pH of the solution is p$Ka_1$ or p$Ka_2$.

of hydrogen evolution reaction. Second, lithium ions should serve as sole charge carriers to avoid complications from proton contribution. The pH of electrolytes should be higher than the p*Ka* values of hydroquinone derivatives.

To prevent dissolution of reduced quinones (phenates) in aqueous electrolytes, which can incur capacity loss, polymerizations were conducted in parallel by reacting halogenated quinones with sodium sulfide.[36,37] The distribution of molecular weight of PBDTDS was determined by matrix-assisted laser desorption/ionization in combination with time of flight mass spectrometer (MALDI-TOF MS).[38] Figure S2 shows that PBDTDS is an oligomer with the number of repeating units ranging from 2 to 8, in agreement with our previous elemental analysis.[37]

Figure 3a shows chemical structures of PAQS and PBDTDS. Compared to their quinone monomers, the difference is the incorporating redox-inactive C–S–C linkers to quinone backbone. Figure 3b and 3c show the significant difference in capacity in neutral (pH 7) electrolytes, corresponding to 120 and 20 mAh g$^{-1}$ for PBDTDS and PAQS, respectively. When the pH of electrolyte increases to 13, the capacity of PBDTDS reaches up to 196 mAh g$^{-1}$ (91.6% of the theoretical capacity), whereas the capacity of PAQS is only 30 mAh g$^{-1}$. When pH is 14, the capacity of PAQS sees a substantial increase, approaching 100 mAh g$^{-1}$. PBDTDS shows a slight decrease in capacity, which may be caused by dissolution of discharged PBDTDS owing to small molecular weight (Figure S3). When the electrolyte is 4 M LiOH, PAQS shows a sharp increase in capacity to 180 mAh g$^{-1}$, in agreement with our previous results.[18] Apparently, neither PBDTDS nor PAQS demonstrate either high capacity or stable cycling when the pHs of electrolytes are lower than the p$Ka_2$ values of the corresponding monomers ($AQH_2$ and $BDTDH_2$). It is worth noting that even though in the case when the pH of electrolytes is slightly higher than p$Ka_2$, both polymers still do not show the best cell performance. For example, although pH 13 and 14 are higher than p$Ka_2$ of $AQH_2$, PAQS shows quite low capacities. We attribute this to the difference between the real p*Ka* values of polyquinones in solid-electrodes and the measured p*Ka* values of quinone monomers in solutions. As there are no available lithium-intercalating cathodes for ALIBs when pH is larger than 13, PAQS is thus excluded to be used as an anode for ALIBs. Instead, PBDTDS demonstrates stable cycling and high capacities in both pH 7 and 13 electrolytes (Figure 3e).

To understand the pH-dependent capacity utilization of polymer electrodes, we compare with aqueous flow batteries. In flow batteries, anthraquinone-based molecules are fully soluble in water and have been reported to show close to 100% capacity utilization independent of pH.[33] It is therefore interesting that the same redox core shows different behaviors in solid versus soluble forms. We hypothesize that this difference may come from unfavorable polymer conformation at low pH that results in limited electrolyte access to the redox sites. When the pH of an electrolyte is less than the p$Ka_1$ of hydroquinone, protons serve as the charge carrier and coordinate with the reduced quinone (Q) to form hydroquinone ($QH_2$). In this scenario, polymer conformation is compact because the polymer chains are electrically neutral and the inter-/intra-chain hydrogen bonding is strong. When the reduction proceeds at higher pH, the reduced quinones adopt the ionic form $Q^{2-}$-$(M^+)_2$ instead. Ionization of the polymer chains weakens those interactions and renders polymer chain extended,[39–41] which results in swelling of polymer particles to allow full penetration of electrolyte to enable electrode reactions take place. As a consequence, more and more redox-active sites in polymers become accessible, thus approaching a higher capacity utilization. In contrast, all quinone molecules in aqueous flow batteries are dissolved in the electrolytes and each redox-active site can be readily accessible to contribute capacity. A detailed study on the relationship of polymer swelling and electrochemical properties in aqueous electrolytes will be reported in the future.

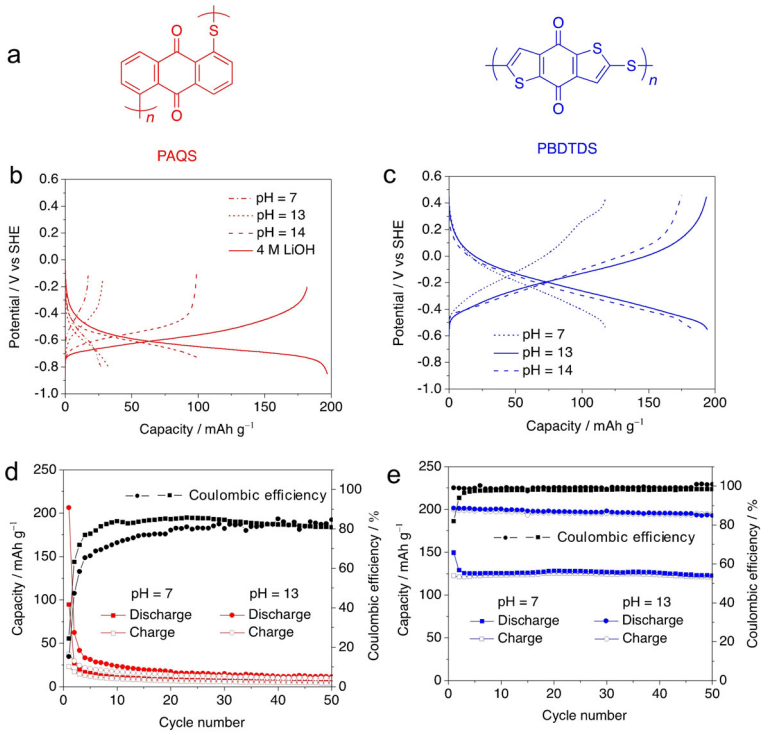


**Figure 3.** Comparison of electrochemical performance between PAQS and PBDTDS. (a) The structures of two poly(quinonyl sulfide)s. (b,c) Voltage profiles for PAQS and PBDTDS in different electrolytes at 1 C rate. (d,e) Cycle stability of both poly(quinonyl sulfide)s at pH 7 and 13 at 1 C. (1 C: 214 mA g$^{-1}$ for PBDTDS, 225 mA g$^{-1}$ for PAQS). Electrolytes: 2.5 M $Li_2SO_4$ (pH 7, 13), 1 M LiOH (pH 14), and 4 M LiOH.

Figure 4a shows the voltage profiles of PBDTDS against varying pHs, which have similar average potentials but gradually increased capacity when pH increases from 7 to 13. The pH dependence of capacity is clearly presented in Figure 4b: the capacity increases from 50 to 196 mAh g$^{-1}$ when pH is increased from 3 to 13. The decreased capacity at pH 14 is a result of the dissolution of discharged PBDTDS (Figure S3). An additional plateau at low pH values is observed (Figures 3c and 4a), which is not expected

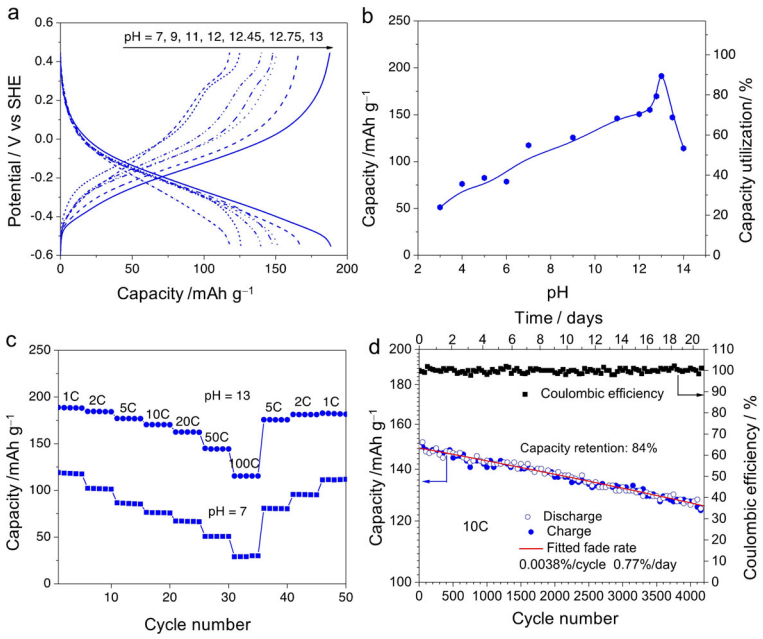


**Figure 4.** The electrochemical performance of PBDTDS. (a) The voltage profiles for the pH from 7 to 13. (b) pH-dependent capacity and capacity utilization at 1 C. (c) The rate performance of PBDTDS at pH 7 and 13. (d) Cycle stability of PBDTDS at pH 13 at 10 C. PBDTDS, super P carbon, and PTFE binder with mass ratios of 3:6:1 for (a), (b), (c), and 6:3:1 for (d) were adopted to prepare composite electrodes. To get fitted fade rates, the cycling result is plotted in semi-log scale (d).

from the redox behavior of the BDTD molecule (Figure S1). A two-step single-electron transfer process in the less swollen polymer at these conditions might be responsible. Electron paramagnetic resonance may be employed to confirm the presence of radicals in the future. Figure 4c shows that PBDTDS has better rate performance at pH 13 over pH 7. For example, at pH 13, the capacity retention (100 C relative to 1 C) is 63.1%; whereas the capacity retention is 25% at pH 7. The difference in rate capability may be related to the distinct charge-transfer resistance ($R_{ct}$) at pH 7 and 13 (Figure S4). PBDTDS shows only 77 Ω of $R_{ct}$ at pH 13, which is less than the half of 166 Ω at pH 7, indicating faster reaction kinetics at pH 13. Our hypothesis is that the partial involvement of $H^+$ in the electrode reaction at low pHs has limited the reaction kinetics in a similar way as it has limited the discharge capacity: the presence of hydrogen bonds formed within the polymer particles at the beginning of the reaction suppresses electrolyte intake, resulting in inferior electrode performance.[34] We note, nonetheless, that the amount of $H^+$ involved in the electrode reaction, even at low pH such as pH 7, is expected to be insignificant, and the electrode may still be considered a $Li^+$-storing. When the reduction of PBDTDS takes place in an unbuffered electrolyte with a pH value smaller than the p$Ka_2$ of BDTD, $H^+$ and $Li^+$ would participate in balancing the negative charges at the reduced quinone units. The consumption of $H^+$ causes the local pH around the surface of PBDTDS particles to increase to pH > p$Ka_2$, making the subsequent charge compensation solely involve $Li^+$ cations. Therefore, in unbuffered near-neutral electrolytes, we expect any protonation to be limited to the surface of the active particles, and any pH change to be local. This situation again contrasts flow batteries: in an unbuffered neutral quinone flow battery, the pH change of the bulk electrolyte could be significant, because concentrated redox-active quinones are dissolved in electrolyte and all subjected to protonation. Even 1% protonation in reduced quinones can incur order-of-magnitudes decrease in proton concentration, leading to an immediate increase in pH of bulk electrolyte.[33]

Figure 4d shows the long-term cycling and PBDTDS demonstrates 84% of capacity retention over 4200 cycles and ≈99.6% of Coulombic efficiency. Through fitting the 21-day cycling results, we found that PBDTDS electrode has fade rates of 0.0038% per cycle and 0.77% per day, respectively. We suspect that the reason behind the capacity fading is mainly a result of the gradual dissolution of reduced PBDTDS. There is no sign of PBDTDS decomposition during the course of cycling.

Choosing $LiCoO_2$ as the cathode, we fabricated a balanced full cell with the configuration of PBDTDS | 2.5 M $Li_2SO_4$ (pH 13) | $LiCoO_2$. Figure 5a shows the

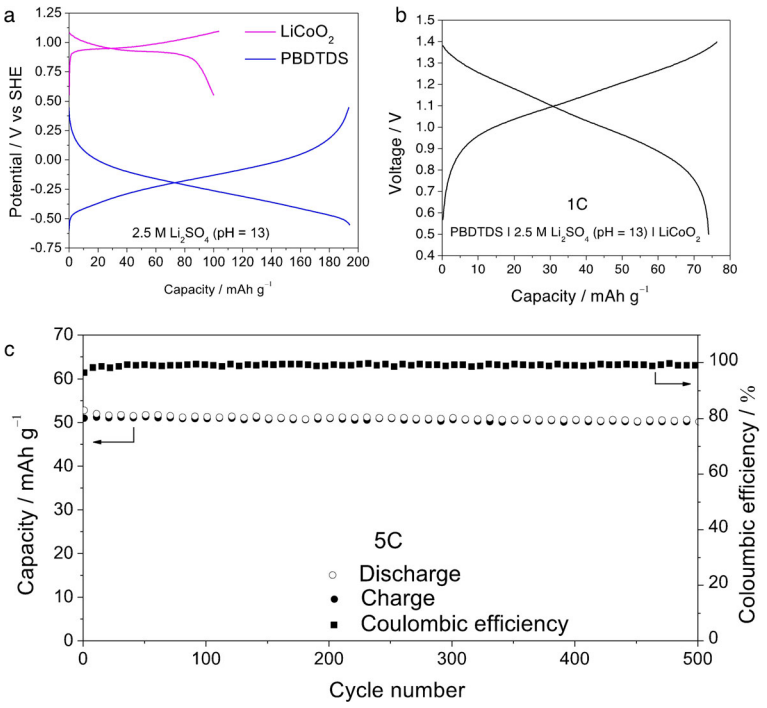


**Figure 5.** A balance full cell with the structure PBDTDS | 2.5 M $Li_2SO_4$ (pH 13) | $LiCoO_2$. (a) The voltage profiles for $LiCoO_2$ and PBDTDS, separately, in a three-electrode cell with Ag/AgCl reference electrode. (b) The voltage profile of the balance full cell. Capacity is calculated based on the combined mass of cathode and anode. (c) Cycle stability of the balance cell at 5 C. PBDTDS, super P carbon, and PTFE binder with mass ratio of 6:3:1 was adopted to prepare composite electrodes.

voltage profiles for both $LiCoO_2$ and PBDTDS at pH 13 using a Ag/AgCl reference electrode. Figure 5b presents the voltage profiles of the full cell, an average discharge voltage of 1.08 V and capacity of 72 mAh $g^{-1}$ based on both electrodes active mass. At 10 C, the full cell shows a capacity of 50 mAh $g^{-1}$ and an average Coulombic efficiency of 99.9%. The capacity loss is negligible over 500 cycles.

In summary, we report a *para*-quinone polymer anode in mild ALIBs. We found that the pH of electrolytes can significantly influence cell performance of quinone-based ALIBs. Only when the pH value of electrolytes is far greater than the p$Ka_2$ values of the corresponding hydroquinone monomers can PBDTDS and PAQS demonstrate the highest capacity and stable cycling. Because of the lower p$Ka_2$ of $BDTDH_2$ than that of $AQH_2$, PBDTDS demonstrates excellent cycling stability and high capacity at pH 13. As a result, we show an ALIB that operates at pH 13 with a voltage of 1.08 V and a capacity of 72 mAh $g^{-1}$ and negligible decay over 500 cycles.

## Experimental Section

### Synthesis of PDBDTDS and PAQS

To a solution of 2,6-dibromobenzo[1,2-b:4,5-b′]dithiophene-4,8-dione or 1,5-dichloroanthraquinone in anhydrous *N*- methyl-2-pyrrolidone in an oven-dried Schlenk flask, anhydrous sodium sulfide was added under argon atmosphere. The resulting mixture was subject to oil bath and heated at 100 °C for overnight. The resulting product was filtrated, washed several times with deionized water and acetone, then dried at 120 °C for 12 h to afford final product.

### Electrochemical measurements.

PBDTDS or PAQS, super P carbon, and polytetrafluoroethylene (PTFE) binder with mass ratios of either 3:6:1 or 6:3:1 were adopted to prepare composite electrodes. Stainless steel mesh (316 grade, 400×400) was used as current collector. Lithium sulfate in water (2.5 M) was prepared and apparent pH of electrolytes were adjusted by adding certain amount of either sulfuric acid or lithium hydroxide. The resulting electrolytes were deaerated through bubbling argon for 30 mins. CR 2032 Coin cell was assembled in the air. Celgard® 3401 was used as separators. Active carbon clothes were used as counter electrodes, Ag/AgCl/saturated KCl was used as reference electrode. The electrochemical measurements were conducted on LAND equipment and biologic electrochemical workstation (VMP3). All tests were carried out at 25 °C. Two-electrode coin cell configuration was employed to evaluate its electrochemical activity at 1 C (214 mA $g^{-1}$) via galvanostatic charge/discharge technique.

## Acknowledgements

*The authors acknowledge the funding support from the Advanced Research Projects Agency-Energy (DE-AR0000380).*

## *Conflict of interest*

*The authors declare no conflict of interest.*

**Keywords:** aqueous batteries · Li-ion batteries · p*Ka* · protons · quinones

[1] N. Shpigel, M. R. Lukatskaya, S. Sigalov, C. E. Ren, P. Nayak, M. D. Levi, L. Daikhin, D. Aurbach, Y. Gogotsi, *ACS Energy Lett.* **2017**, *2*, 1407 – 1415.
[2] D. G. Kwabi, K. Lin, Y. Ji, E. F. Kerr, M.-A. Goulet, D. De Porcellinis, D. P. Tabor, D. A. Pollack, A. Aspuru-Guzik, R. G. Gordon, M. J. Aziz, *Joule* **2018**, *2*, 1894 – 1906.
[3] Y. Liang, Y. Yao, *Joule* **2018**, *2*, 1690 – 1706.
[4] L. Jiang, Y. Lu, C. Zhao, L. Liu, J. Zhang, Q. Zhang, X. Shen, J. Zhao, X. Yu, H. Li, X. Huang, L. Chen, Y.-S. Hu, *Nat. Energy* **2019**, *4*, 495 – 503.
[5] X. Ji, *Energy Environ. Sci.* **2019**, *12*, 3203 – 3224.
[6] X. Wu, Y. Qi, J. J. Hong, Z. Li, A. S. Hernandez, X. Ji, *Angew. Chem. Int. Ed.* **2017**, *56*, 13026 – 13030; *Angew. Chem.* **2017**, *129*, 13206 – 13210.
[7] J. Huang, Z. Guo, Y. Ma, D. Bin, Y. Wang, Y. Xia, *Small Methods* **2019**, *3*, 1800272.
[8] S. Perticarari, T. Doizy, P. Soudan, C. Ewels, C. Latouche, D. Guyomard, F. Odobel, P. Poizot, J. Gaubicher, *Adv. Energy Mater.* **2019**, *9*, 1803688.
[9] W. Li, J. R. Dahn, D. S. Wainwright, *Science* **1994**, *264*, 4.
[10] H. Kim, J. Hong, K. Y. Park, H. Kim, S. W. Kim, K. Kang, *Chem. Rev.* **2014**, *114*, 11788 – 11827.
[11] Y. Wang, J. Yi, Y. Xia, *Adv. Energy Mater.* **2012**, *2*, 830 – 840.
[12] Z. Liu, Y. Huang, Y. Huang, Q. Yang, X. Li, Z. Huang, C. Zhi, *Chem. Soc. Rev.* **2020**, *49*, 180 – 232.
[13] J. Y. Luo, W. J. Cui, P. He, Y. Y. Xia, *Nat. Chem.* **2010**, *2*, 760 – 765.
[14] R. Ruffo, C. Wessells, R. A. Huggins, Y. Cui, *Electrochem. Commun.* **2009**, *11*, 247 – 249.
[15] Q. Qu, L. Fu, X. Zhan, D. Samuelis, J. Maier, L. Li, S. Tian, Z. Li, Y. Wu, *Energy Environ. Sci.* **2011**, *4*, 3985.
[16] M. Pasta, C. D. Wessells, R. A. Huggins, Y. Cui, *Nat. Commun.* **2012**, *3*, 1149.
[17] G. Wang, L. Fu, N. Zhao, L. Yang, Y. Wu, H. Wu, *Angew. Chem. Int. Ed.* **2007**, *46*, 295 – 297; *Angew. Chem.* **2007**, *119*, 299 – 301.
[18] Y. Liang, Y. Jing, S. Gheytani, K. Y. Lee, P. Liu, A. Facchetti, Y. Yao, *Nat. Mater.* **2017**, *16*, 841 – 848.
[19] D. Sun, Y. Tang, K. He, Y. Ren, S. Liu, H. Wang, *Sci. Rep.* **2015**, *5*, 17452.
[20] D. Sun, X. Xue, Y. Tang, Y. Jing, B. Huang, Y. Ren, Y. Yao, H. Wang, G. Cao, *ACS Appl. Mater. Interfaces* **2015**, *7*, 28337 – 28345.
[21] S. Muench, A. Wild, C. Friebe, B. Haupler, T. Janoschka, U. S. Schubert, *Chem. Rev.* **2016**, *116*, 9438 – 9484.
[22] Q. Zhao, Z. Zhu, J. Chen, *Adv. Mater.* **2017**, *29*, 1607007.
[23] S. Perticarari, E. Grange, T. Doizy, Y. Pellegrin, E. Quarez, K. Oyaizu, A. J. Fernandez-Ropero, D. Guyomard, P. Poizot, F. Odobel, J. Gaubicher, *Chem. Mater.* **2019**, *31*, 1869 – 1880.
[24] X. Dong, L. Chen, J. Liu, S. Haller, Y. Wang, Y. Xia, *Sci. Adv.* **2016**, *2*, e1501038.
[25] L. Chen, W. Li, Z. Guo, Y. Wang, C. Wang, Y. Che, Y. Xia, *J. Electrochem. Soc.* **2015**, *162*, A1972 – A1977.
[26] K. Lin, R. Gómez-Bombarelli, E. S. Beh, L. Tong, Q. Chen, A. Valle, A. Aspuru-Guzik, M. J. Aziz, R. G. Gordon, *Nat. Energy* **2016**, *1*, 16102.
[27] S. Gheytani, Y. Liang, F. Wu, Y. Jing, H. Dong, K. K. Rao, X. Chi, F. Fang, Y. Yao, *Adv. Sci.* **2017**, *4*, 1700465.
[28] M. Park, E. S. Beh, E. M. Fell, Y. Jing, E. F. Kerr, D. Porcellinis, M. A. Goulet, J. Ryu, A. A. Wong, R. G. Gordon, J. Cho, M. J. Aziz, *Adv. Energy Mater.* **2019**, *9*, 1900694.
[29] L. Tong, Y. Jing, R. G. Gordon, M. J. Aziz, *ACS Appl. Energy Mater.* **2019**, *2*, 4016 – 4021.
[30] M. Quan, D. Sanchez, M. F. Wasylkiw, D. K. Smith, *J. Am. Chem. Soc.* **2007**, *129*, 12847 – 12856.
[31] L. Sieuw, A. Jouhara, E. Quarez, C. Auger, J. F. Gohy, P. Poizot, A. Vlad, *Chem. Sci.* **2019**, *10*, 418 – 426.
[32] Y. Ji, M. A. Goulet, D. A. Pollack, D. G. Kwabi, S. Jin, D. Porcellinis, E. F. Kerr, R. G. Gordon, M. J. Aziz, *Adv. Energy Mater.* **2019**, *9*, 1900039.
[33] S. Jin, Y. Jing, D. G. Kwabi, Y. Ji, L. Tong, D. De Porcellinis, M.-A. Goulet, D. A. Pollack, R. G. Gordon, M. J. Aziz, *ACS Energy Lett.* **2019**, *4*, 1342 – 1348.
[34] W. Choi, D. Harada, K. Oyaizu, H. Nishide, *J. Am. Chem. Soc.* **2011**, *133*, 19839 – 19843.

[35] Y. Liang, P. Zhang, S. Yang, Z. Tao, J. Chen, *Adv. Energy Mater.* **2013**, *3*, 600 – 605.
[36] Z. Song, H. Zhan, Y. Zhou, *Chem. Commun.* **2009**, 448 – 450.
[37] Y. Jing, Y. Liang, S. Gheytani, Y. Yao, *Nano Energy* **2017**, *37*, 46 – 52.
[38] A. P. Gies, W. K. Nonidez, M. Anthamatten, R. C. Cook, J. W. Mays, *Rapid Commun. Mass Spectrom.* **2002**, *16*, 1903 – 1910.
[39] L. Brannon-Peppas, N. A. Peppas, *Chem. Eng. Sci.* **1991**, *46*, 715 – 722.
[40] V. Yadav, A. V. Harkin, M. L. Robertson, J. C. Conrad, *Soft Matter* **2016**, *12*, 3589.
[41] V. Yadav, Y. A. Jaimes-Lizcano, N. K. Dewangan, N. Park, T.-H. Li, M. L. Robertson, J. C. Conrad, *ACS Appl. Mater. Interfaces* **2017**, *9*, 44900 – 44910.

Manuscript received: January 13, 2020
Revised manuscript received: February 12, 2020
Accepted manuscript online: February 25, 2020
Version of record online: ■■ ▮▮, 0000

**pKa dependent capactiy:** Given that quinone-based batteries are heavily influenced by the pH of electrolytes, we studied the influence of acid dissociation constants (p*K*a) of hydroquinones on their performance as electrode materials for aqueous lithium-ion batteries. At pH 13, poly(anthraquinonyl sulfide) demonstrates a low capacity and poor cycle life, whereas poly(benzo[1,2-b:4,5-b′]dithiophene-4,8-dione-2,6-diyl sulfide) demonstrates a capacity of 196 mAh $g^{-1}$ and fade rates of 0.0038% per cycle over 4200 cycles, 0.77% per day over 21 days; the differences in capacity and cycle stability can be explained by the difference of corresponding p*K*a values.

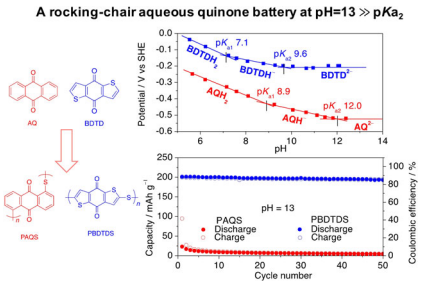


*Y. Jing, Y. Liang, S. Gheytani, Y. Yao**

■■ – ■■

**A Quinone Anode for Lithium-Ion Batteries in Mild Aqueous Electrolytes**




**These are not the final page numbers! ↗↗**